EUROFUSION WPS1-PR(16) 15968

P Kornejew et al.

Density measurements at fusion experiments: two-color versus dispersion interferometers

Preprint of Paper to be submitted for publication in
Review of Scientific Instruments

This work has been carried out within the framework of the EUROfusion Consortium and has received funding from the Euratom research and training programme 2014-2018 under grant agreement No 633053. The views and opinions expressed herein do not necessarily reflect those of the European Commission.

Density measurements at fusion experiments: two-color versus dispersion interferometers

P. Kornejew[1]*, H. Dreier[1,2,4], A. Solomakhin[3], M. Hirsch[1]

[1]Max-Planck-Institut für Plasmaphysik, EURATOM Association, Wendelsteinstr. 1, 17491 Greifswald, Germany

[2] Forschungszentrum Jülich GmbH, Association EURATOM-FZ Jülich, Institut für Plasmaphysik, Trilateral Euragio Cluster, 52425 Jülich, Germany

[3] Budker Institute of Nuclear Physics, Novosibirsk 630090, Russia

[4] now: Gesellschaft für Anlagen- und Reaktorsicherheit, Schwertnergasse 1, 50667 Köln, Germany

*Email: petra.kornejew@ipp.mpg.de

Two different types of interferometers, used for the measurement of the electron density in fusion experiments, are compared. The challenges due to mechanical vibrations of the optical components can be addressed by a conventional two-color interferometer or by a dispersion interferometer. We perform here a direct comparison of these two methods, showing that the dispersion interferometer is superior to the two-color interferometer. Although the dispersion interferometer is much more robust, one must nonetheless address of a number of issues, some of which are shared with the two-color interferometer. These include the use of a corner cube reflector and also the significant impact of ambient air turbulence and temperature and humidity changes. The error of the integrated line density, caused by air fluctuations on the time scale of several seconds, was found to be $\pm 4.5 \cdot 10^{17}$ m^{-2} for the dispersion interferometer and $\pm 2.5 \cdot 10^{18}$ m^{-2} for the two-color interferometer. At the time scale of less than one second, the data noise is smaller by a factor of about 5-10 for both interferometers, allowing investigations of the influence of vibrations of the corner cube reflector with amplitudes up to 65 µm. The two-color interferometer compensates for these by a factor of 0.001. We will show that the small residual vibration noise (0.0005 of the initial value) for the dispersion interferometer originates from disturbances of the CO_2 laser by back reflections from the corner cube reflector into the laser. This can be avoided by the increasing distance between the incident and reflected beams at the corner cube reflector to five times the radius of the beam waist. In order to reduce the noise due to thermal air effects, the interferometer should be covered, and components heated by the laser radiation must be cooled.

I. Introduction

At Wendelstein 7-X (W7-X) as at other fusion devices, interferometry is an important diagnostic for measuring the line-integrated electron density[1, 2, 3, 4], one of the key parameters of the fusion plasma. It is required for machine control and for the calibration of the density profiles measured by Thomson scattering. In order to deliver reliable and accurate data, the interferometer needs to be able to cope with mechanical vibrations and perturbations due to time-varying ambient effects such as air temperature and air humidity. Due to the space requirements of superconducting coils and the large cryostat of W7-X, the interferometer features path lengths of up to 20 m from the interferometer bench to the corner cube reflector (CCR) at the inboard side of the torus (outside the vacuum vessel) and back. In addition, the

corner cube reflector cannot be mounted on the same support structure as the other interferometer components. This could lead to significant thermal changes of the mechanical laser input path length (about1 mm $\approx 100 \cdot \lambda_{CO_2}$) in comparison to the reference path. These thermal drifts and further mechanical vibrations require precise compensation to ensure that the line-integrated density can be measured to an accuracy of about $1 \cdot 10^{18} \mathrm{m}^{-2}$ (≈ 0.01 fringes at 10 µm).

Moreover, future long term discharges of up to 30 minutes put very strong requirements on the stability of the interferometer.

This paper explores two possible interferometer designs for the use at W7-X: 1) a CO_2/CO two-color interferometer[5] and 2) a dispersion interferometer[6].

The first laboratory tests of the two-color laser interferometer are presented in section II. The basic set-up is discussed there, as are the main challenges with this type of interferometer. In order to study the influence of slow thermal movements of optical components, the CCR was positioned on a manual translation stage. Additionally, a piezo vibration stage was added between the CCR and its mount. This setup allows the separate investigation of the impact of slow translations of up to 1 mm and higher frequency vibrations (20 and 70 Hz) with an peak-to-peak amplitude of up to 65 µm. The tests are performed in both directions, parallel and perpendicular to the beam path. The first tests of a dispersion interferometer at a fusion device delivered promising experimental results at TEXTOR[6]. The principal set-up of this interferometer will be explained in section III. The test procedure is exactly the same as for the two-color interferometer. Although these show significant advantages of the dispersion interferometer in comparison to the two-color system, limits with respect to the use of CCRs are demonstrated and explained separately in section IV.

Since the long path length at fusion experiments cannot be avoided and air conditions cannot be easily controlled around large plasma devices, it will be shown in section V that temperature drifts and air convection limit the accuracy of both interferometers significantly and must be taken into account.

The results of the study presented in this paper are summarized in section VI.

II. Setup and vibration compensation tests of the two-color interferometer

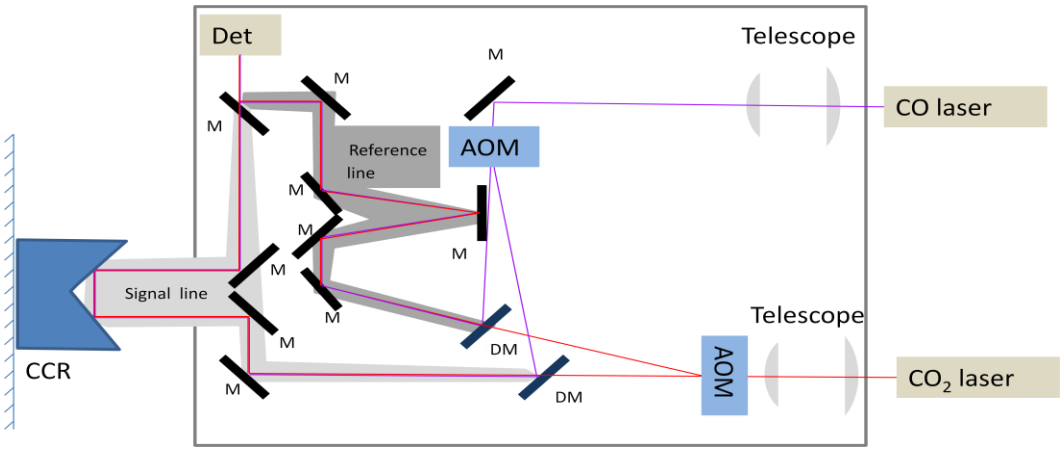

FIG. 1. Schematic of the laboratory setup of the two-color interferometer

The two-color interferometer originally planned for W7-X was designed to use wavelengths in the infrared region that would produce phase shifts of less than 2π at high plasma densities up to $10^{20}\,m^{-2}$. A CO_2 laser interferometer with a wavelength of 10.6 µm was combined with a CO laser interferometer (λ=5.3 µm) to compensate for mechanical drifts and vibrations. The interferometer setup is shown in FIG. 1 Both Mach-Zehnder interferometers feature spatially separated signal and reference lines of the same length. Passing an acousto-optic modulator (AOM), the reference beam (1^{st} harmonic) is generated from the CO_2 laser beam (0^{th} harmonic), being deflected by the sound waves of the AOM crystal under a certain angle and shifted in frequency by the frequency of the acoustice waves. A different AOM driver frequency is used interferometer (40 MHz for 10.6µm and 25 MHz for 5.3 µm) to avoid electrical crosstalk and to enable the use of a single detector, the signal from which is analyzed digitally. Thus, one fewer beam splitter is required, in comparison to a two-detector scheme. Nevertheless, the two wavelengths must be combined by means of a dichroic mirror that totally reflects one wavelength while being transparent to the second. Vibrations of the dichroic mirror contribute only to the phase shift of the reflected beam. Thus, it cannot be compensated by any way. Furthermore, the separation into reference and signal line happens in each AOM at a distance of about 1 m before the wavelengths are combined. Different air properties (temperature, convection) in the volumes between the AOM and the beam combiners can significantly affect the signal/noise ratio. The significant spatial separation between signal and reference line that is unavoidable at large fusion experiments, could also add another source of errors; the different air conditions in the two volumes passed by signal and reference beams introduce an additional phase shift that varies on the scale of several seconds. These effects will be analyzed separately in section V. To simulate future torus hall conditions with the laboratory set-up (FIG. 1), the CCR was mounted to a wall well separated from the main optical components of the interferometer bench.

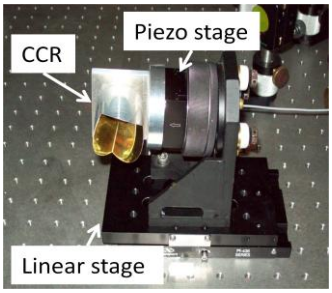

FIG. 2. Experimental setup of the CCR for testing the compensation of drifts and vibrations in the direction perpendicular to the laser beams

The ability of the two-color interferometer to compensate for mechanical drifts was tested by mounting the CCR on a manual linear stage, as shown in FIG. 2. Investigating directions both parallel and perpendicular to the beam, it was found in both cases that the system compensates for these movements by a factor of 0.001.

Mounting a piezo stage between the CCR and its mechanical mount (see FIG. 2), vibration well defined in amplitude (up to 65 µm) and frequency (20 and70 Hz) can be applied to the CCR.

For the laser propagation through the plasma in the region far from the cutoff frequency, as is the case for $\lambda = 5-10\mu m$ and electron densities of $n_e \leq 10^{21} m^{-3}$, it can be shown that the phase shift due to the plasma[7] is given by $\Delta\varphi_{Plasma} = \frac{\lambda e^2}{4\pi c^2 \varepsilon_0 m_e} \int n_e(z) dz$, where e is the elementary charge, c the speed of light, m_e the mass of the electron, ε_0 the dielectric constant of vacuum, n_e the electron density of the plasma, z the plasma length and λ the laser wavelength. The phase changes at both wavelengths are extracted from the detector signal and the trigger of the AOM driver delivered by means of digital data processing using a field programmable gate array (FPGA)[8]. Since $\Delta\varphi_i$ is the sum of the phase shifts at a given wavelength due to changes of the path length and to changes of the electron density $\Delta\varphi_i = \frac{2\pi}{\lambda_i}\Delta z + \frac{\lambda_i e^2}{4\pi c^2 \varepsilon_0 m_e} \int \Delta n_e(z) dz$. The final line-integrated electron density can be obtained from the phase shifts at the two wavelengths

$$\int \Delta n_e(z) dz = \frac{4\pi c^2 \varepsilon_0 m_e}{e^2} \frac{\Delta\varphi_1 \lambda_1 - \Delta\varphi_2 \lambda_2}{\lambda_1^{\,2} - \lambda_2^{\,2}} \qquad (1)$$

where the contribution from changes of the path length Δz cancels out.

The strategy behind is that the longer wavelength is more sensitive to the electron density whereas the shorter wavelength enables a geometry correction. The success of this compensation is checked experimentally.

Results

In the FIG. 3 and FIG. 4, the results of the vibration compensation are plotted. The resolved data streams show that the compensated signal. In the case of vibrations of the CCR with a peak-to-peak amplitude of 65 µm parallel to the beam, the phase shift of the CO_2 interferometer is equal 12.8 fringes, corresponding to a change of the line integrated electron density of $2.7 \cdot 10^{21} m^{-2}$. After compensation with the CO interferometer (FIG. 3), a residual signal corresponding to an integral density of $\pm 1 \cdot 10^{18} m^{-2}$ is measured. This means that vibration compensation is successful only to a certain degree, namely to 1/1000th of the amplitude of the single CO_2 interferometer interference signal. The amplitude of the modulation of the compensated signal due to vibrations significantly exceeds the noise on the time scale of <<1s (FIG. 3b), but it is comparable with the drift of the signal over several seconds (FIG. 3a).

In the case of vibrations of the CCR perpendicular to the laser beams, the compensated signal should not show any modulation if the wavefronts of signal and reference beam are coplanar with one another on the detector. This is difficult to achieve, especially in the case of long path lengths when over which large number of beam-guiding optics disturb the wave fronts. Furthermore, the center of mass of the CCR could not be placed exactly on the axis of the piezo. As a result, an additional movement parallel to the laser beams could not be avoided completely. The residual modulation of the compensated signal due to the vibration is found

to be only slightly above the noise level on the time scale of << 1 s and negligible for t>1 s. Drifts due to air dynamics dominate the noise level on that time scale and lead to a significant error of $\pm 3 \cdot 10^{18} m^{-2}$.

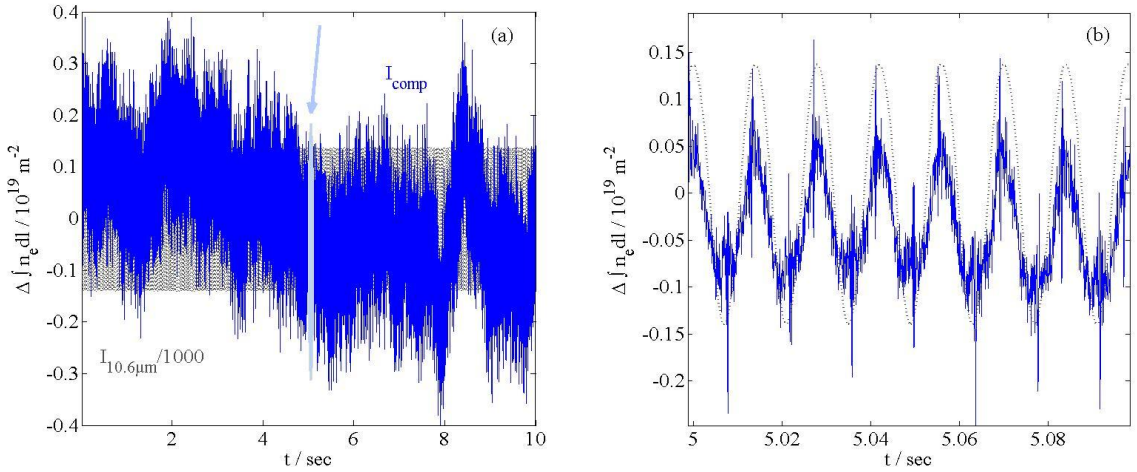

FIG. 3. Compensated and uncompensated phase shifts at different time scales, expressed in terms of the corresponding change of the integrated electron density, due to vibrations of the CCR parallel to the laser beam direction. The phase shift of the CO_2 interferometer (after subtracting the constant offset and dividing by 1000) is given in grey, the compensated signal calculated from Eq. (1) in blue. The time window shown in (b) is marked in (a) in light blue.

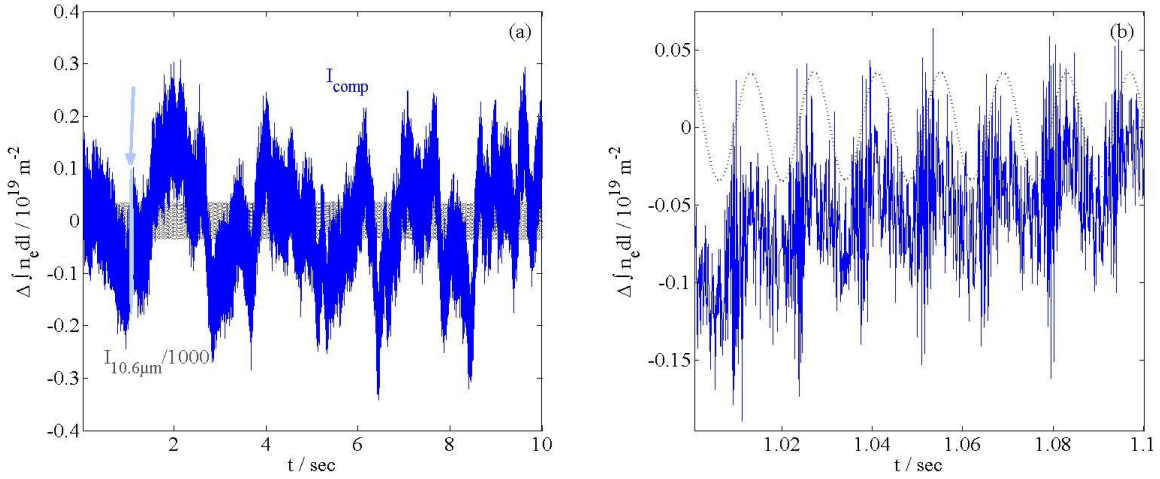

FIG. 4. Unresolved (a) and resolved (b) signals in the case of vibrations of the CCR perpendicular to the laser beam direction. The signal of the CO_2 interferometer divided by 1000 is given in grey, the compensated signal calculated from formula (1) in blue. The time window shown in (b) is marked in (a) in light blue.

III. Setup and vibration compensation tests of the dispersion interferometer

A detailed description of the dispersion interferometer (DI) at TEXTOR was given in references[6, 9, 10] For testing the sensitivity of the dispersion interferometer (DI), one of the DI modules at TEXTOR is examined in the laboratory. The same CCR unit (FIG. 2) was placed

behind the exit of the DI modules. The distance of the CCR is chosen to be 5.5 m to match conditions for density measurements at TEXTOR. A schematic of the setup is shown in FIG. 5.

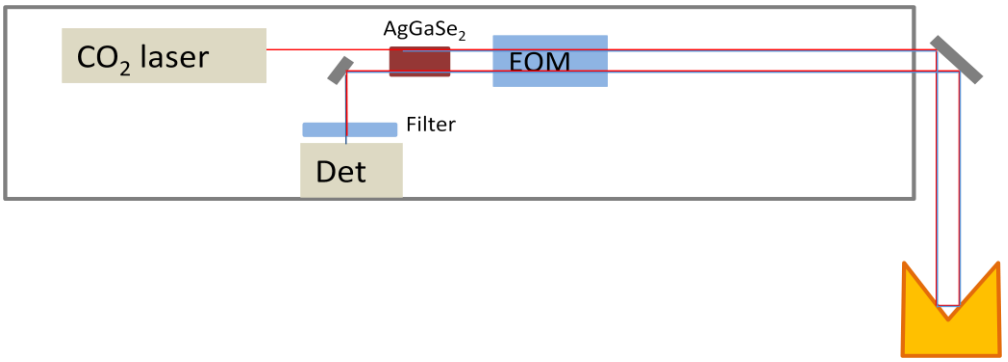

FIG. 5. Setup of the dispersion interferometer

The beam of the CO_2 laser is focused into an $AgGaSe_2$ non-linear crystal where it becomes partially frequency-doubled. The generated second harmonic (5.3 µm) and the fundamental (10.6 µm) beams then travel together through the plasma to a CCR that reflects them back, parallel to the incident beam offset by a certain distance. Passing the $AgGaSe_2$ crystal a second time, another 5.3 µm beam is generated from the fundamental one. After the residual 10.6 µm radiation is blocked by a sapphire plate, both 5.3 µm beams are focused onto the detector:

$I = A_1^2 + A_2^2 + A_1 A_2 \cos(\Delta\phi)$, where A_1^2 and A_2^2 are the amplitudes of the two interfering 5 µm beam and $\Delta\phi$ - the phase shift between both. The line-intergrated electron density n_e is calculated from the phase shift $\Delta\phi$.

The phase shift due to the plasma can be described by

$$\Delta\phi_{Plasma} = 2\frac{\lambda_L e^2}{4\pi c^2 \varepsilon_0 m_e}\int n_e dl - \frac{\lambda_L/2\, e^2}{4\pi c^2 \varepsilon_0 m_e}\int n_e dl = \frac{3}{2}\frac{\lambda_L e^2}{4\pi c^2 \varepsilon_0 m_e}\int n_e dl \qquad (2)$$

with $\lambda_L = 10.6\mu m$.

As the second harmonic is polarized perpendicular to the first harmonic, an additional phase shift is introduced only to one of the beams by using an electro-optical modulator (EOM). This results in the final expression for the measured overall phase shift

$$\Delta\phi = \cos(\Omega t) + \frac{3}{2}\frac{\lambda_L e^2}{4\pi\varepsilon_0 m_e c^2}\int n_e dl \qquad (3)$$

where Ω is the frequency of the modulator.

The completely identical beam path of the interfering beams leads to several advantages of the DI when compared with the two-color interferometer:

- Mechanical drifts and vibrations parallel to the beam path cancel out – that is,

$\Delta\phi_{mech} = 2\frac{2\pi}{\lambda_L}\Delta z - \frac{2\pi}{\lambda_L/2}\Delta z = 0$. Consequently, the compensation for vibrations of all optical elements parallel to the optical path is intrinsic.

- The full dynamic range of the data acquisition system can be spent on the plasma induced phase shift. (In the case of the two-color system less than 10 percent of the overall phase shift is due to the plasma; the major part of the dynamic range is required for mechanical effects.)
- No separate reference line, which could give rise to significant noise due to additional air effects, is required. Only second order effects resulting from the difference of the indices of refraction of air at the two wavelength can play a role.

Results

The data measured while performing slow movements of the CCR are shown in FIG. 6.

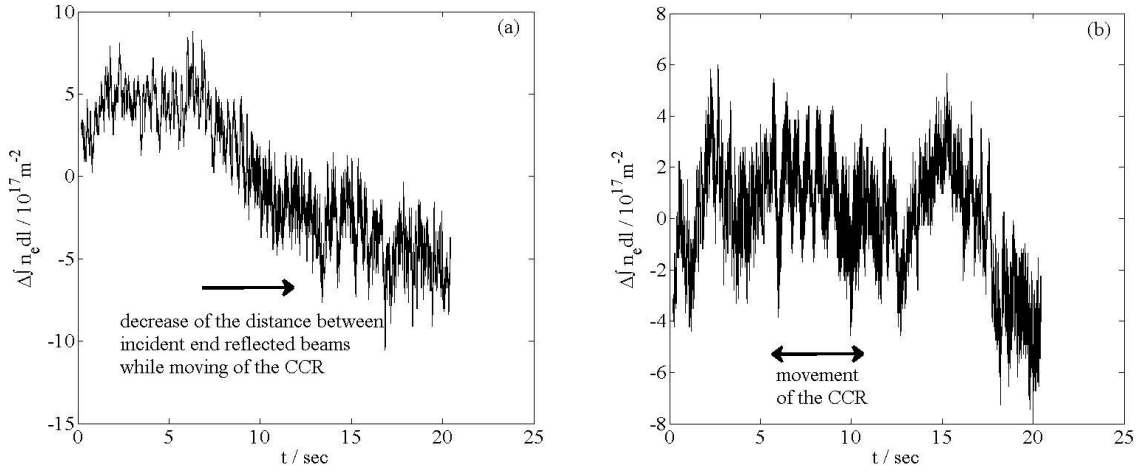

FIG. 6. Line-integrated densities correspond to the measured phase shifts before, during and after moving the CCR 1 mm perpendicular (a) and parallel (b) to the laser beam path. The bold arrows marks the time interval of the movement.

Movements of the CCR perpendicular to the beam path (FIG. 6a) over 1 mm lead to a substantial drift $\Delta n_e = 7 \cdot 10^{17} m^{-2}$ due to changes of the path length through dispersive element (modulator) impairing the alignment of the reflected laser beam. This results in an additional phase shift which can easily be verified by taking into account the geometrical characteristics (distances and focal lengths) of the interferometer. Additionally, a marginal increase of the noise level appears due to the misalignment. The impact of the movement parallel to the optical path is small in comparison with the noise of $\sigma_{n_e}^{DI} = \pm 5 \cdot 10^{17} m^{-2}$ on the time scale $\Delta t \geq 1\text{sec}$ (FIG. 6b).

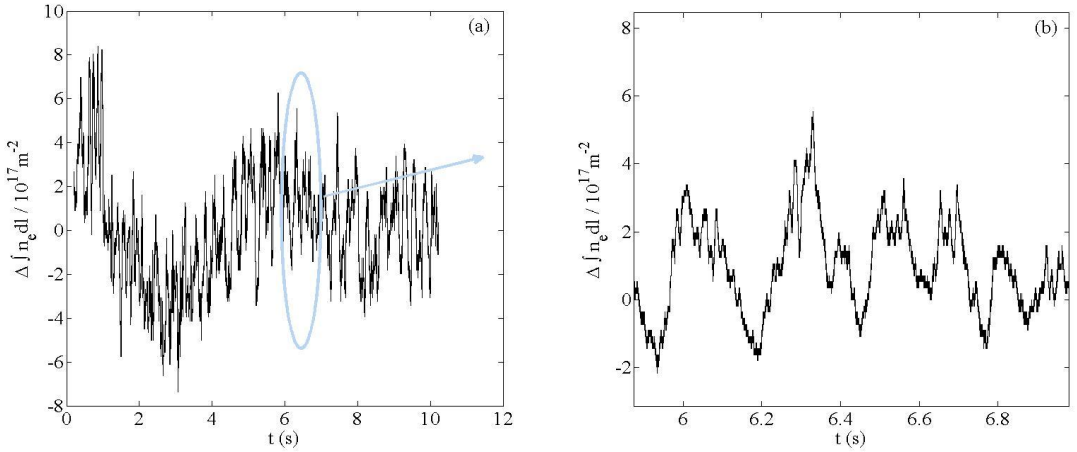

FIG. 7. Line integrated densities corresponding to the measured phase shifts for the case of an unperturbed CCR (without vibrations and movements).

It can be seen from FIG. 8 that the signal variation introduced by the traverse vibrations of the CCR is much smaller than the drift of the signal over several seconds (FIG. 8a) and is also of the same order as the noise without vibrations (FIG. 8b).

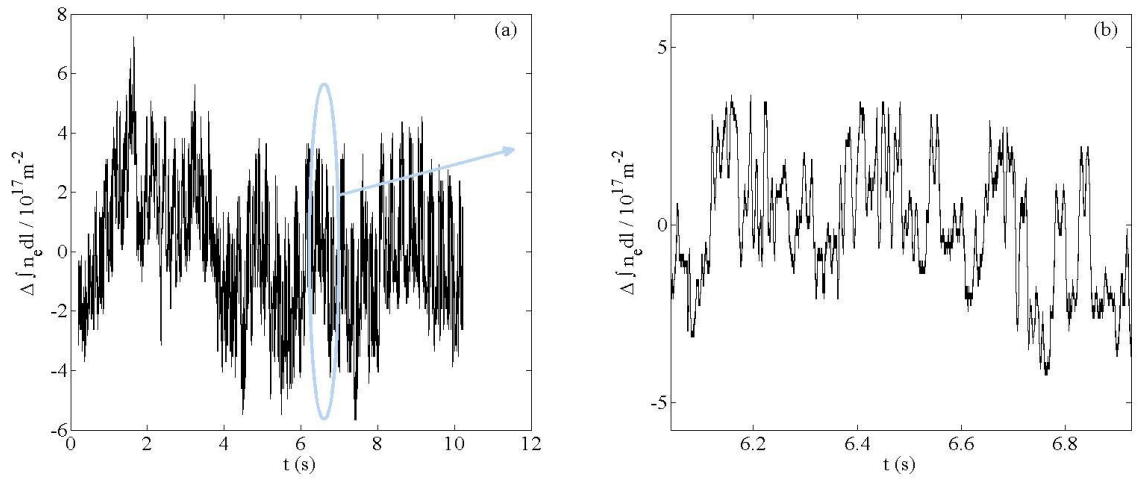

FIG. 8: Line integrated densities corresponding to the measured phase shifts for the case of vibrations with a peak-to-peak amplitude of 65 µm to the CCR perpendicular to the laser beams. FIG. 8b shows a fraction of the whole time trace as marked in (a)

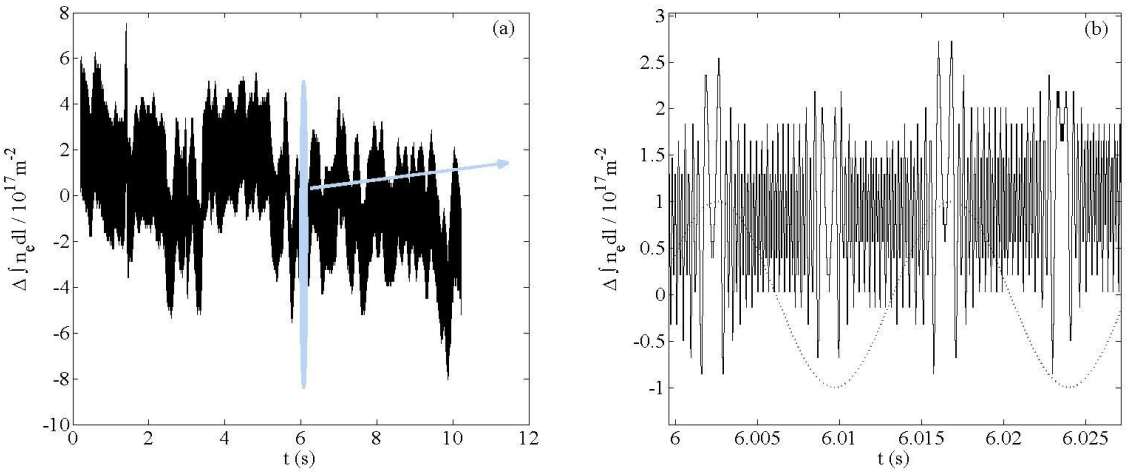

FIG. 9. (a) Line-integrated densities corresponding to the measured phase shifts due to vibrations of the CCR with a peak-to-peak amplitude of 65 µm and a frequency of 60 Hz parallel to the laser beams. (b) A fraction of the time trace, with a 60 Hz sine wave overlaid for better understanding.

When vibrations of the CCR are introduced parallel to the beam path, the noisy time trace over several seconds (FIG. 9a), but the time-resolved signal (FIG. 9b) is clearly modulated at the frequency of the vibrations.

Nevertheless, this effect is smaller than that measured with the two-color interferometer at least by a factor of two. Moreover, this modulation looks different, resembling to a frequency modulation in the form $I \propto \sum_i \alpha_i \sin(\sin(i \cdot \Theta t))$, where Θ is the frequency of the vibrations.
We will analyze this in detail in the following section.

IV. Impact of the beam reflected from the CCR on the stability of the CO_2 laser

CO_2 lasers, on which both types of interferometer are based, are very sensitive to back reflections from the experiment into the laser resonator. If a small fraction of the laser radiation is reflected back on the laser axis, it becomes amplified in the resonator and leads to an additional component of the laser beam shifted in phase dependending on the distance of the source of the back reflection and its velocity (drifts, vibrations).
That is why, when using CCRs which return the beam exactly parallel to the incident beam, a possible impact of the reflected beam on the laser operation has to be taken into account.

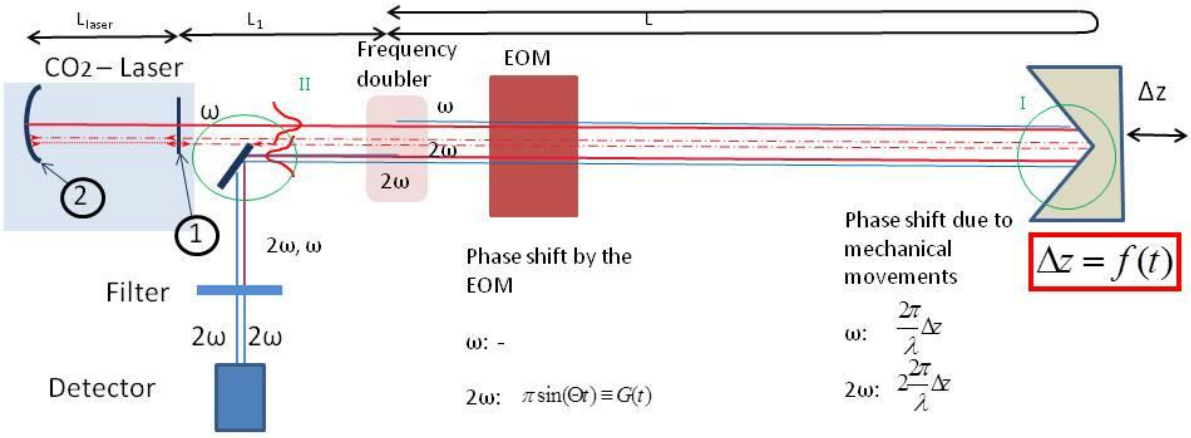

FIG. 10. Principle components of the DI and processes resulting in a modulated density signal (see FIG. 9). The optical elements responsible for a possible impact of the beam reflected from the CCR on the stability of laser operation are marked with green circles.

In the DI tested, the distance between reflected and incident beams was limited in order to guarantee the second pass through the frequency doubling crystal.

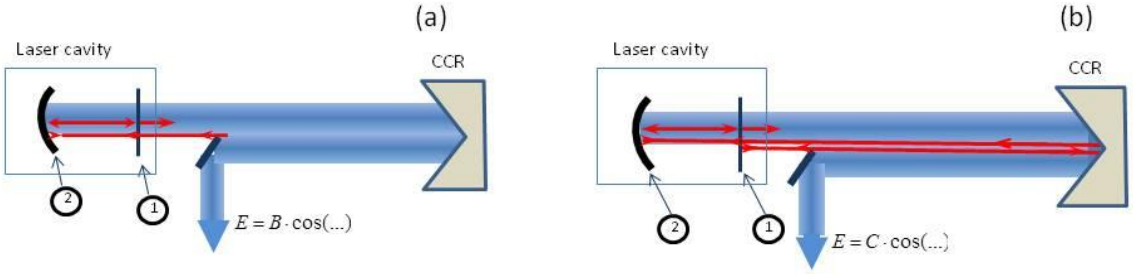

FIG. 11: Additional resonator cavities due to the partial overlap of incident and reflected beam at the CCR (red lines). Arrows show the beam direction, light red arrows mark the principal reflections. The resonator mirrors of the laser surfaces are marked with (1) and (2).

It will be shown now that the insufficient distance is the reason why the laser output appears partially modulated in phase depending on the frequency of the vibrations applied to the CCR. As a consequence, the electron density calculated from the interference signal will also be modulated (FIG. 9b). The principle of this effect is shown in FIG. 10 and FIG. 11.

During one reflection from the CCR, the vibration $f(t)$ of the piezo causes further phase shifts to both interfering beams $2\frac{2\pi}{\lambda_L} f(t)$ and $2\frac{2\pi}{\lambda_L/2} f(t)$.

If the distance between the 10.6 µm-beam reflected from the CCR and the incident beam is not sufficient large, it will not be possible to separate both beams completely by the half mirror (II in FIG. 10) and some part of the reflected beam will return into the laser resonator, where it will become amplified and finally will be part of the laser output frequency modulated depending on $f(t)$.

By this way, both interfering 5.3-µm beams will consist of three components:

The main component originates from the frequency doubled unperturbed laser radiation generated in the resonator cavity (FIG. 10) and leads to two second harmonic beams at the detector, with amplitudes $A_{1,2}$ respectively.

Because of the overlap of the wings of the beam reflected from the CCR and the incident beam, both beam cannot be separated completely by the half mirror (FIG. 10). A small part of the reflected 10.6 µm radiation finds its way back to the outcouppling mirror (1), where it partially enters the laser, becomes amplified, exits the laser as a part of the laser beam and will cross the whole interferometer path ones more. Than, it reaching the detector with amplitude $B_{1,2}$ (FIG. 11) with an additional phase shift

$$\Delta\varphi_B = \varphi_{Pl}^{10} - 2\frac{2\pi}{\lambda_L}\left(2L_1 + 2L_{Laser} + L + f(t)\right) = \varphi_{Pl}^{10} - \varphi - F(t) + \varphi_B. \qquad (4)$$

Here, the phase shift of the first harmonic due to the plasma is φ_{Pl}^{10} and φ, $F(t)$ and φ_B are defined by $\varphi \equiv \frac{4\pi}{\lambda_L} L$, $F(T) \equiv \frac{4\pi}{\lambda_L} f(t)$ and $\varphi_B \equiv \frac{4\pi}{\lambda_L}\left(2L_1 + 2L_{Laser}\right)$.

L is the path length of the interferometer, L_1 the path length between the frequency doubling crystal (FDC) and the outcouppler and L_{Laser} the length of the laser resonator.

The third component originates from a reflection at outer surface of the outcouppler returning to the laser cavity across the whole interferometer path, transmitting the outcouppler and becoming amplified (FIG. 11b). It exits the laser, passes the interferometer path a third time with the final amplitudes $C_{1,2}$ and the additional phase shift

$$\Delta\varphi_C = 2\varphi_{Pl}^{10} - 2\frac{2\pi}{\lambda_L}\left(2L_1 + L + f(t) + 2L_1 + 2L_{Laser} + L + f(t)\right) = 2\varphi_{Pl}^{10} - 2\varphi - 2F(t) + \varphi_c, \qquad (5)$$

with the constant phase shift $\varphi_C \equiv \frac{4\pi}{\lambda_L}\left(4L_1 + 2L_{Laser}\right)$. Obviously, the intensity of the main component exceeds that of the other both by much more than an order of magnitude

$$\begin{aligned} A_{1,2} &>> B_{1,2}, \\ A_{1,2} &>> C_{1,2} \end{aligned} \qquad (6)$$

The resulting field strength of the two interfering beams at the detector are given by equations (7) and (8) where E_1 is the electrical field strength of the second harmonic generated during the first pass through the frequency doubling crystal (FDC), E_2 describes the 5.3 µm beam generated during the second pass through the FDC. λ_L is the laser

wavelength. In the electro-optical modulator (EOM), $G(t)=\pi\sin(\Theta t)$ is added to the phase of the second harmonic.

$$\begin{aligned}E_1 &= A_1\cos\left(2\omega t+G(t)+\varphi_{Pl}^{5}-\varphi-F(t)\right)\\ &+B_1\cos\left(2\omega t+G(t)+\varphi_{Pl}^{5}+\varphi_{Pl}^{10}-2\varphi-2F(t)+\varphi_B\right)\\ &+C_1\cos\left(2\omega t+G(t)+\varphi_{Pl}^{5}+2\varphi_{Pl}^{10}-3\varphi-3F(t)+\varphi_C\right)\end{aligned} \quad (7)$$

and

$$\begin{aligned}E_2 &= A_2\cos\left(2\omega t+\varphi_{Pl}^{10}-\varphi-F(t)\right)\\ &+B_2\cos\left(2\omega t+2\varphi_{Pl}^{10}-2\varphi-2F(t)+\varphi_B\right)\\ &+C_2\cos\left(2\omega t+3\varphi_{Pl}^{10}-3\varphi-3F(t)+\varphi_C\right).\end{aligned} \quad (8)$$

Calculating the intensity on the detector $I=(E_1+E_2)^2$ and taking into account that the detector cannot follow the fast oscillation of the laser ω and that all slow varying components (which argument of the cosine not contains G(t)) blocked by a high pass filter, $\bar{I}$ results in

$$\begin{aligned}\bar{I} &= \overline{(E_1+E_2)^2}\\ &=(A_1A_2+B_1B_2+C_1C_2)\cos\left(G(t)+\Delta\varphi_{Pl}\right)\\ &+(A_1B_2+A_2B_1)\cos(G(t)+\Delta\varphi_{Pl})\cos(2\varphi_{Pl}^{10}-\varphi-F(t)+\varphi_B)\\ &+(A_1B_2-A_2B_1)\sin(G(t)+\Delta\varphi_{Pl})\sin(2\varphi_{Pl}^{10}-\varphi-F(t)+\varphi_B)\\ &+(A_1C_2+A_2C_1)\cos(G(t)+\Delta\varphi_{Pl})\cos(4\varphi_{Pl}^{10}-2\varphi-2F(t)+\varphi_C)\\ &+(A_1C_2-A_2C_1)\sin(G(t)+\Delta\varphi_{Pl})\sin(4\varphi_{Pl}^{10}-2\varphi-2F(t)+\varphi_C)\\ &+(B_1C_2+B_2C_1)\cos(G(t)+\Delta\varphi_{Pl})\cos(2\varphi_{Pl}^{10}-\varphi-F(t)+\varphi_C-\varphi_B)\\ &+(B_1C_2-B_2C_1)\sin(G(t)+\Delta\varphi_{Pl})\sin(2\varphi_{Pl}^{10}-\varphi-F(t)+\varphi_C-\varphi_B)\end{aligned} \quad (9)$$

This expression can be written in the form of:

$$\bar{I}=D_1\cos\left(G(t)+\Delta\varphi_{Pl}\right)+D_2\sin(G(t)+\Delta\varphi_{Pl})=\sqrt{D_1^{\,2}+D_2^{\,2}}\cos\left(G(t)+\Delta\varphi_{Pl}+\chi\right) \quad (10)$$

with

$$\begin{aligned}D_1 &= (A_1A_2+B_1B_2+C_1C_2)+(A_1B_2+A_2B_1)\cos(2\varphi_{Pl}^{10}-\varphi-F(t)+\varphi_B)\\ &+\left(A_1C_2+A_2C_1\right)\cos(4\varphi_{Pl}^{10}-2\varphi-2F(t)+\varphi_C)\\ &+(B_1C_2+B_2C_1)\cos(2\varphi_{Pl}^{10}-\varphi-F(t)+\varphi_C-\varphi_B)\end{aligned} \quad ,$$

$$\begin{aligned}D_2 &= (A_1B_2-A_2B_1)\sin(2\varphi_{Pl}^{10}-\varphi-F(t)+\varphi_B)\\ &+(A_1C_2-A_2C_1)\sin(4\varphi_{Pl}^{10}-2\varphi-2F(t)+\varphi_C)\\ &+(B_1C_2-B_2C_1)\sin(2\varphi_{Pl}^{10}-\varphi-F(t)+\varphi_C-\varphi_B)\end{aligned}$$

and $\tan(\chi)=\dfrac{D_2}{D_1}$.

The data processing procedure of the DI is described in reference[11]. Expression 10 differs from the case of the DI without any impact of the reflected beam where the filtered signal has the form of

$$\bar{I} = A_1 A_2 \cos\left(G(t) + \Delta\varphi_{Pl}\right) \quad .$$

After normalizing, the line integrated electron density was determined from the time of the zero-crossing of $\cos\left(\Delta\varphi_{Pl} + G(t)\right)$:

$$G(t_0) + \Delta\varphi_{Pl} - \chi = \frac{\pi}{2} \tag{11}$$

Obviously, the error of the determined plasma phase shift is given by χ . In our laboratory tests without plasma, the phase shift yields (taking into account relation 6):

$$\chi \cong \frac{(A_2B_1 - A_1B_2)\sin(\varphi + F(t) - \varphi_B) + (A_2C_1 - A_1C_2)\sin(2\varphi + 2F(t) - \varphi_C)}{A_1A_2} \tag{12}$$

In the case of a linear function $f(t) = v \cdot t$, the calculated $\int n_e dl$ -equivalent error and the measured time trace are shown in FIG. 12. Thus, the oscillations observed in the experiment can be reproduced by fitting the parameters $\frac{(A_2B_1 - A_1B_2)}{A_1A_2}, \frac{(A_2C_1 - A_1C_2)}{A_1A_2}$ and the velocity v to the measured data. FIG. 12(a) shows the fit and the data in the case of parallel movements of the CCR using the translation stage. The residual discrepancy is caused by the data noise (see FIG. 12(b)) and the slightly non-constant velocity of the CCR (manual operation of the translation stage). Similarly, the model function can be fitted to the measured modulations of the signal in the case of vibrations induced to the CCR by a piezo actuator assuming $f(t) = a \cdot \sin(\Omega t)$ (FIG. 13). Although the data are dominated by noise and drifts of the signal due to air effects, modulations due to impact of the reflected from the CCR beam to the laser are not negligible. The amplitude of the modulation depends only on the distance between incident and reflected beams, assuming an accurate positioning of the half mirror (II (green) in FIG. 10). Additional laboratory tests showed that a distance between both beams should be at least 5 times the radius of the 10.6µm-beam waist at the CCR. A partial or complete overlap of incident and reflected beams at the CCR would always lead to crucial disturbance of the laser stability. This should always be taken into account while using a CCR in the CO_2 interferometer setup.

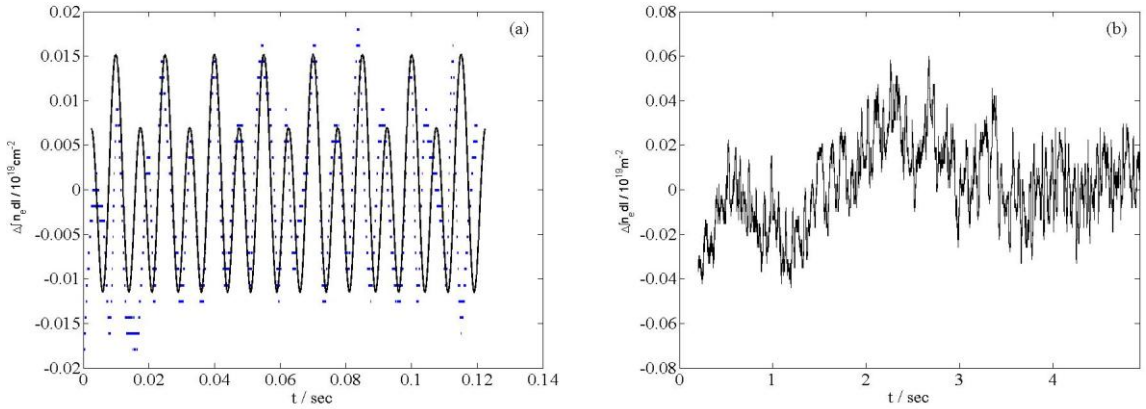

FIG. 12. (Color online) (a) Fit of the calculated modulation function to the measured signals (dashed line) during slow translation of the CCR parallel to the laser beams. The fit parameters were found to be $\frac{(A_2B_1 - A_1B_2)}{A_1A_2} = 0.006$, $\frac{(A_2C_1 - A_1C_2)}{A_1A_2} = 0.016$, $v = 1.8\frac{m}{s}$; (b) shows the typical noise without movement of the CCR.

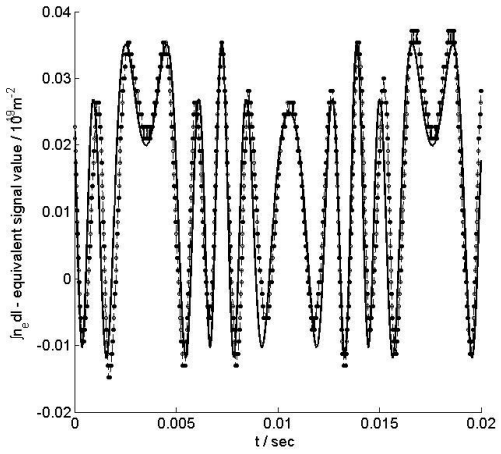

FIG. 13. (Color online) Measured data (dashed line) and fit of the calculated modulation function to the density derived from the measured signals during vibration of the CCR parallel to the laser beams in the case of vibrations induced by a piezo. The parameters of the piezo were set to $\Omega = 70Hz$ (frequency) and $a = 10.7\mu m$ (peak-to-peak-amplitude).

For experimental reasons, in the used set-up of the DI, the axis of the EOM was not exactly parallel to the polarization of the second harmonic, leading to an additional modulation of the first harmonic, only with a different amplitude $G_1(t) = k_1 \sin(\Omega t) \neq G_2(t) = k_2 \sin(\Omega t)$. In this case, the resultant impact on the calculated electron density looks more complex. Nevertheless, it could be shown that it also has the form of $a \cdot \cos(f) + b \cdot \cos(2 \cdot f)$.

Not only the planar outcouppling mirror of the laser can induce back reflections into the laser resonator, but also every other planar optical element. This has to be taken into account in the alignment procedure.

Limitations of large scale interferometers by thermal air effects

When using an interferometer in experiments with a large beam path, the measured electron density (neglecting vibrations) will be affected by both drifts of the air parameters (temperature, pressure and humidity) and air turbulences, due to differences in the dispersion indices at 5.3 and 10.6 µm. Especially, if the electron density must be measured over several minutes, temperature and humidity of the air passed through by the laser beams must be kept constant over that time. Let us consider changes of the differences of the indices of reflection of both wavelength for typical parameters of the air p=1000 *hPa*, T=20°*C* and *H*=80%, 10%. Calculating $\Delta\varphi = [\Delta n_5 - \Delta n_{10}]\frac{2\pi}{\lambda_L} 2L$ using data published by R.J. Mathar[12] it can be seen that the air pressure changes (FIG.14a) can be neglected, while changes of the air temperature (FIG.14b) and the humidity (FIG.14c) result in significant phase change. Small changes of the ambient temperature of about $\Delta T = 0.8K$ at 80% humidity or of the humidity $\Delta H = 4\%$ lead to changes of the measured line integrated electron density of about $10^{18} m^{-2}$ if the path length in air of the interferometer is assumed to be one meter; n_5 and n_{10} are the indices of refraction of the wavelengths 5.3 and 10.6 μm respectively, and $\lambda_L = 10.6\mu m$ is the wavelength of the laser. FIG.14b demonstrates that the impact of temperature change is much larger in moist air than in dry air.

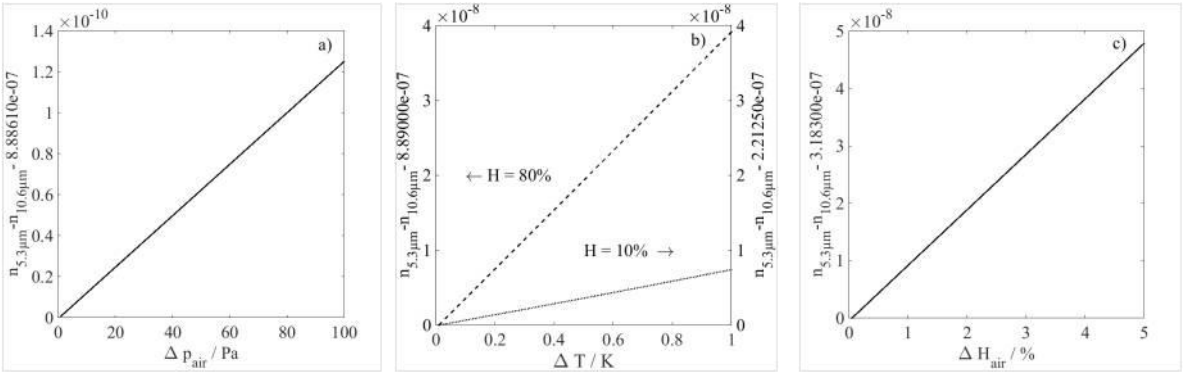

FIG.14. Difference of the indices of refraction of humid air (80% humidity) at a pressure of 1000 *hPa* and a temperature of 20°C for the interferometer wavelength 5.3 and 10.6 μm as a function of (a) pressure changes, (b) temperature changes and (c) humidity changes.

Furthermore, air convection due to components warmed by the laser (attenuators, shutters, beam dumps absorbing nuisance reflections from optical surfaces) lead to refraction of the beams that varies with wavelength. Especially if the gradient of the temperature is nearly perpendicular to the beam, these effects are significant. A simple model can be used to estimate their order of magnitude. Let us assume a flow of heated moist air (ΔT=0.1*K*) nearly parallel to the laser beams with ambient air parameters p_{air}=1000 *hPa*, T_{air}=20 °*C* and *H*=80%. The index of refraction decreases with increasing temperature. For incident angles larger a certain value $\theta > \theta_{total}$ the beam becomes reflected from the vertical convection flow of warm air (total internal reflection). Thus, under the assumed conditions the beams become deflected in under slightly different angles for both wavelength leading to a small change of the length of the beam path – different for $\lambda_{5\mu m}$ and $\lambda_{10\mu m}$. Because of the difference of the index of refraction at 10.6 μm and 5.2 μm an additional phase shift of about 0.01fringes is measured corresponding to changes in the line integrated electron density of up to

$\Delta\int n_e dl \cong 1\cdot 10^{18} m^{-2}$ (assuming the deflection of the whole beam and a path length through air of 1*m*). For longer path length (l>>1*m*) even the partial deflection of the beams (different distortion of the wave fronts) induces a signal noise of some $10^{17} m^{-2}$ as can be seen in the measured data of the DI.
These effects have to be considered for two-colour interferometers and for dispersion interferometers. Additionally, for the two-color interferometer the region before combining both laser beams after the AOM is much more sensitive because every of the four beams (two harmonics, two wavelength) travel through different air volumes.
In any case, the noise and the drifts of both interferometers seem to be determined by fluctuations of air so that it appears to be necessary that components heated by the laser are equipped with a cooling system keeping the temperature differences inside the interferometer below 1*K*.

V. Summary

The aim of this paper was the direct comparison of the two-color interferometer with the DI in order to find the most qualified diagnostic for the determination of the electron density at W7-X. Both interferometers were tested using the same laboratory set-up. Well defined vibrations were applied to the most critical of the optical components: the CCR. Slow translations of the CCR with amplitudes up to 1 mm were performed using a manual stage. The measurements showed that on a time scale $\Delta t << 1s$ the two-color interferometer compensates the additional noise introduced by the vibrations of the CCR up to 1/1000 of the response of a single CO_2 interferometer. The vibration compensation by the DI was found to be at least two times better.
Furthermore, the pattern of the small residual vibration noise of the DI was shown to be caused by the insufficient distance between incident and reflected beams at the CCR, leading to a slight modulation of the laser wavelength. It could be removed by changing the beam geometry at the CCR, namely by increasing the distance between the beams to a value larger than at least 5 times the radius of the 10.6 µm beam waist at this position.
When not actively perturbed, the noise of the two-color interferometer corresponded to an error in the integrated line density of $\sigma_{n_e}^{2col} = 5\cdot 10^{17} m^{-2}$ and respectively for the DI $\sigma_{n_e}^{DI} = 1.5\cdot 10^{17}\,\mathrm{m}^{-2}$, demonstrating again the decisive superiority of the DI.
Investigating the signals for larger time scales $\Delta t \geq 1\,\mathrm{s}$, the noise of both interferometers becomes dominated by fluctuations of the ambient temperature. In this case as well, the measured errors of the integrated line density were much smaller for the DI ($5\cdot 10^{17} m^{-2}$) than for the two-color interferometer ($2.5\cdot 10^{18} m^{-2}$). The reason for the significantly lower noise level of the DI is the common beam path of the interfering beams. Nevertheless, it exceeded the noise for $\Delta t << 1s$ significantly. This needs to be considered when setting up the interferometer at W7-X; namely, all optical components will need to be protected by a cover against transient air flows of the torus hall. Components, heated by the laser radiation, must be cooled carefully.

VI. Acknowledgement

This work has been carried out within the framework of the EUROfusion Consortium and has received funding from the Euratom research and training programme 2014-2018 under grant agreement No 633053. The views and opinions expressed herein do not necessarily reflect those of the European Commission.

References

[1] K. Tanaka, A. L. Sanin, L. N. Vyacheslavov, T. Akiyama, K. Kawahata, T. Tokuzawa, Y. Ito and S. Okajima, Rev. Sci. Instrum. **75**, 3429 (2004

[2] P. Acedo et al., Rev. Sci. Instrum. **75**, 4671 (2004)

[3] P. Innocente, Rev. Sci. Instrum. **74**, 3625 (2003)

[4] M. Sánchez and J. Sánchez, Rev. Sci. Instrum. **76**, 046104 (2005)

[5] P. Kornejew et al., Rev. Sci. Instrum. **77**, 10F128 (2006)

[6] Bagryanski, P. A.,Khilchenko, A. D., Kvashnin, A. N., Lizunov, A. A., Voskoboynikov, R. V., Solomakhin, A. L., Koslowski, H. R., TEXTOR, Team, Rev. Sci. Instrum. **77**, 053501 (2006)

[7] D. Véron, Submilimeter Interferometry of High-Density Plasmas, Infrared and millimeter waves, **2**, ed. by K. J. Button, Academic Press (1979)

[8] L. Esteban, M. Sánchez, J. Sánchez, P. Kornejew, M. Hirsch, J.A. López, A. Fernández and O. Nieto-Taladriz, Fusion Science and Technology, **58**, 771 (2010)

[9] A Lizunov, P Bagryansky, A Khilchenko, Yu V Kovalenko, A Solomakhin, W Biel, H T Lambertz, Yu Krasikov, M Mitri, B Schweer, H Dreier, Rev. Sci. Instrum. **79,** 10E708 (2008)

[10] H Dreier, P Bagryansky, N Baumgarten, W Biel, H T Lambertz, M Lehnen, A Lizunov, A Solomakhin, Rev. Sci. Instrum. **82**, 063509 (2011)

[11] A. D. Khil'chenko et al., Instruments & Experimental Techniques;May2009, Vol. 52 Issue 3, p382

[12] R. J. Mathar, "Refractive index of humid air in the infrared: Model fits," J. Opt. A.: Pure Appl. Opt. 9(5), pp. 470–476, 2007